Bioorganic Chemistry 150 (2024) 107554

Contents lists available at ScienceDirect

Bioorganic Chemistry

journal homepage: www.elsevier.com/locate/bioorg

Amphiphilic coumarin-based probes for live-cell STED nanoscopy of plasma membrane

Hana Kokot [a], Boštjan Kokot [a], Anja Pišlar [b], Hana Esih [b], Alen Gabrič [b], Dunja Urbančič [b,c], Rojbin El [c], Iztok Urbančič [a,c], Stane Pajk [b,*]

[a] Jožef Stefan Institute, Jamova cesta 39, SI-1000 Ljubljana, Slovenia
[b] University of Ljubljana, Faculty of Pharmacy, SI-1000 Ljubljana, Slovenia
[c] Weatherall Institute of Molecular Medicine, University of Oxford, OX3 9DS Oxford, United Kingdom

ARTICLE INFO

Keywords:
Membrane probe
Fluorescence
STED
Two-photon excitation
Photostability

ABSTRACT

Plasma membranes are vital biological structures, serving as protective barriers and participating in various cellular processes. In the field of super-resolution optical microscopy, stimulated emission depletion (STED) nanoscopy has emerged as a powerful method for investigating plasma membrane-related phenomena. However, many applications of STED microscopy are critically restricted by the limited availability of suitable fluorescent probes. This paper reports on the development of two amphiphilic membrane probes, **SHE-2H** and **SHE-2N**, specially designed for STED nanoscopy. **SHE-2N**, in particular, demonstrates quick and stable plasma membrane labelling with negligible intracellular redistribution. Both probes exhibit outstanding photostability and resolution improvement in STED nanoscopy, and are also suited for two-photon excitation microscopy. Furthermore, microscopy experiments and cytotoxicity tests revealed no noticeable cytotoxicity of probe **SHE-2N** at concentration used for fluorescence imaging. Spectral analysis and fluorescence lifetime measurements conducted on probe **SHE-2N** using giant unilamellar vesicles, revealed that emission spectra and fluorescence lifetimes exhibited minimal sensitivity to lipid composition variations. These novel probes significantly augment the arsenal of tools available for high-resolution plasma membrane research, enabling a more profound exploration of cellular processes and dynamics.

1. Introduction

Plasma membranes (PM) are intricate assemblies of lipids and proteins that act as a barrier between cells and their surroundings. Beyond their essential role as a protective barrier, these dynamic structures play a crucial part in numerous biological processes, including signalling, muscle contraction, cellular uptake, and cell migration, among others. Many of these processes involve significant changes in the membrane's morphology, which thus provides valuable information about a plethora of molecular and biochemical processes in cells and tissues, beyond cell division and cell death[1,2]. Consequently, visualizing the PM is of paramount importance, even when it is not the primary focus of research.

Fluorescence microscopy stands out as a cornerstone technique in the realm of PM research. Furthermore, the scientific landscape in this domain has witnessed a profound transformation in the recent decades, driven by the rapid development of super-resolution techniques, which have ushered in an era of nanoscale investigations[3,4]. Among these techniques, stimulated emission depletion (STED) nanoscopy stands out as the fastest and is particularly well-suited for live-cell research[5,6]. Another advanced fluorescence microscopy technique – two-photon excitation (2PE) microscopy – exploits longer excitation wavelengths and threshold-limited absorption to reduce photodamage, improve optical sectioning, and limit the effect of absorption and scattering in biological tissues[7]. Due to this, it enables imaging deeper in the sample, complementing information obtained by super-resolution microscopy, and is thus commonly used for imaging thick, strongly scattering samples, such as biological tissues *ex vivo*, as well as *in vivo*[8,9]. However, the effectiveness of such methods, similarly to other fluorescent imaging techniques, heavily relies on the performance of fluorescent probes. Several constraints limit the selection of suitable probes [10,11]. Firstly, the excitation and emission spectra of the probes must match the available excitation and detection options of the imaging system, as well as the spectra of other probes in the system. Furthermore,

* Corresponding author.
E-mail address: stane.pajk@ffa.uni-lj.si (S. Pajk).

https://doi.org/10.1016/j.bioorg.2024.107554
Received 26 March 2024; Received in revised form 30 May 2024; Accepted 9 June 2024
Available online 10 June 2024

the probes must exhibit high brightness and photostability. Additionally, for STED microscopy, the emission spectrum of the probe must match the wavelength of the STED laser[12], and for 2PE, the probe's molecular structure, which determines its two-photon cross-section, governs the suitability of a probe[13]. Moreover, for compatibility with live-cell 2PE- and STED nanoscopy, PM probes must be non-toxic and have to exclusively label the PM with little to no distribution to the inner membranes or organelles[14].

Various methods have been employed for the fluorescent labelling of PM. One approach involves the use of fluorescently labelled lectins, such as wheat germ agglutinin, which offers stable PM labelling without any dispersion into intracellular organelles[15]. However, the success of this labelling method is contingent upon the cell type and the specific oligosaccharides present on the outer leaflet of the PM. Furthermore, it is worth noting that the labelled proteins are considerably larger in size compared to molecular probes – 50 kDa compared to 1 kDa – which can restrict the achievable resolution when utilizing super-resolution techniques[15]. Another promising, but so far rarely applied avenue in PM labelling is the application of conjugated polymers, which can provide stable labelling[16]. In contrast, molecular probes continue to dominate as the primary choice for PM labelling in live-cell STED nanoscopy due to their high brightness and photostability, versatility, and small size [11]. However, a significant issue with molecular probes is their lack of specificity, often leading to their redistribution from the PM to other cellular membranes of internal organelles[17]. In general, small molecular probes that offer stable PM labelling typically consist of a lipophilic part embedded in the lipid bilayer and a charged polar head. Short polyethylene glycol linkers or small hydrophilic dendrimers have also been successfully utilized[17,18]. Recently, probes based on a "clickable" zwitterionic anchor and cyanine or squaraine dyes have shown promising results for stable PM staining[19,20]. The advantage of this design strategy is its easy applicability to other types of fluorophores.

In our recent study, we investigated the compatibility of several membrane probes with live-cell STED nanoscopy[21]. Among the probes, the coumarin-based probe **MePyr500** emerged as the most effective, exhibiting high brightness and photostability, noticeable resolution improvement in STED microscopy, and minimal toxicity to cells. However, **MePyr500** exhibited rapid redistribution from the PM to intracellular membranes. In this article, we present the results of the second development phase of the **MePyr500** probe. Since the probe's solubility was not an issue, we extended the aliphatic chains and crucially added additional charge to the polar headgroup to produce two new probes: **SHE-2H** with a zwitterionic configuration and **SHE-2N** with a double positive charge at the polar headgroup (Fig. 1). Both probes enable live-cell STED nanoscopy and 2PE microscopy, and **SHE-2N** very slowly redistributes to intracellular membranes and organelles.

2. Results and discussion

2.1. Synthesis

The synthetic pathway to probes **SHE-2H** and **SHE-2N** is presented in Scheme 1. Briefly, synthesis begins by reacting 3-methoxyaniline with undecan-2-one in the presence of $InCl_3$ to give compound **1**. In the subsequent step, nitrogen of 1,2-dihydroquinoline moiety of compound **1** is methylated to yield compound **2**. The methoxy ether group of compound **2** is then cleaved using BBr_3, resulting in the formation of phenol **3**. A formyl group is introduced at position 2 of phenol **3** through a Vilsmeier-Haack reaction, leading to the production of salicylic aldehyde **4**. Subsequently, salicylic aldehyde **4** undergoes Knoevenagel condensation with methyl 2-(pyridin-4-yl)acetate, resulting in the formation of coumarin **5**. To create the probe **SHE-2H**, the pyridine moiety of compound **5** is alkylated using 1,3-propane sultone. Alternatively, compound **6** is synthesized by alkylating the pyridine group of compound **5** with 1,3-dibromopropane. Finally, the probe **SHE-2N** is formed by reacting compound **6** with trimethylamine.

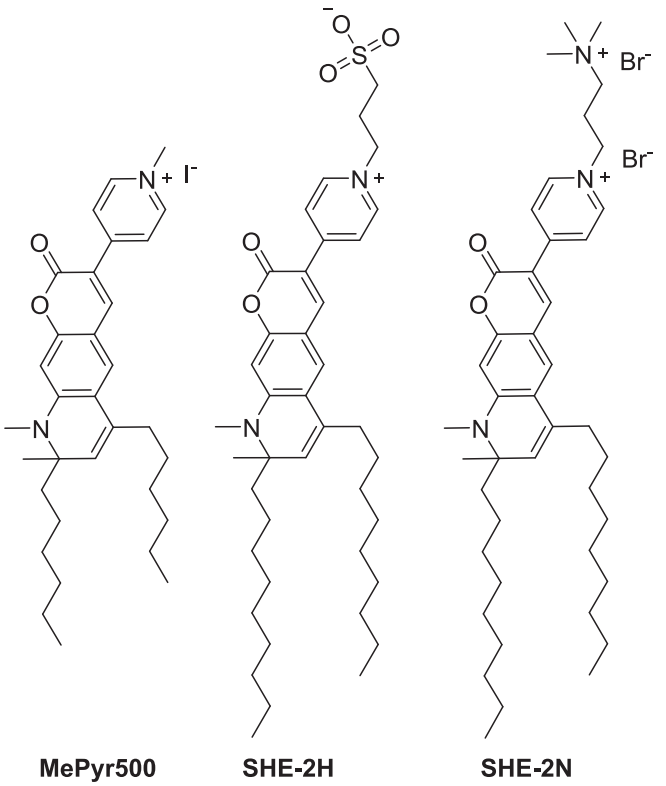

Fig. 1. Structure of probes **MePyr500**, **SHE-2H** and **SHE-2N**.

2.2. Uv–vis absorption and emission spectra

The absorption and emission spectra of **SHE-2N** exhibit a slight red-shift compared to **SHE-2H** and **MePyr500**, despite all compounds sharing the same fluorophore core, as illustrated in Fig. 2. This variation in spectral characteristics is likely attributable to differences in the polar headgroup and counterions associated with each compound. Absorption and emission spectra were also recorded in PBS buffer containing 0.02% polysorbate 80, a non-ionic surfactant (see Supplementary Data, Figure S1). Assuming that the bromide or iodide counterions exchanged with anions from the PBS buffer, the similarity of spectral maxima in both solvents indicates that the red-shift of **SHE-2N** is the consequence of the headgroup.

There was also a noticeable difference in the relative quantum yields in ethanol solution, which were 0.36 for **SHE-2H** and 0.07 for **SHE-2N**. The lower quantum yield observed for **SHE-2N** may be attributed to the quenching effect of bromide counterions[22]. It is likely that the actual quantum yield for **SHE-2N** closely resembles that of **SHE-2H**. This hypothesis is supported by the comparison of spectra for all three probes recorded in ethanol and in PBS buffer containing 0.02% polysorbate 80 (see Supplementary Data, Figures S2, S3, and S4). The **SHE-2H** probe exhibited practically the same intensity in both media, whereas **SHE-2N** and **MePyr500** produced much stronger emission in PBS buffer containing 0.02% polysorbate 80 compared to ethanol solution, with the effect being more pronounced for **SHE-2N**. Both probes, **SHE-2N** and **MePyr500**, have counterions (bromide and iodide) known to quench fluorescence. However, during microscopy, this should not be a problem since counterions can exchange with anions present in the cell medium.

2.3. Cell labelling and probe distribution

To test the suitability of the newly synthesized probes for live-cell microscopy, we incubated them with LA-4 cells and first monitored the labelling efficiency and distribution into the inner cellular structures. During the incubation, cells were constantly being monitored both

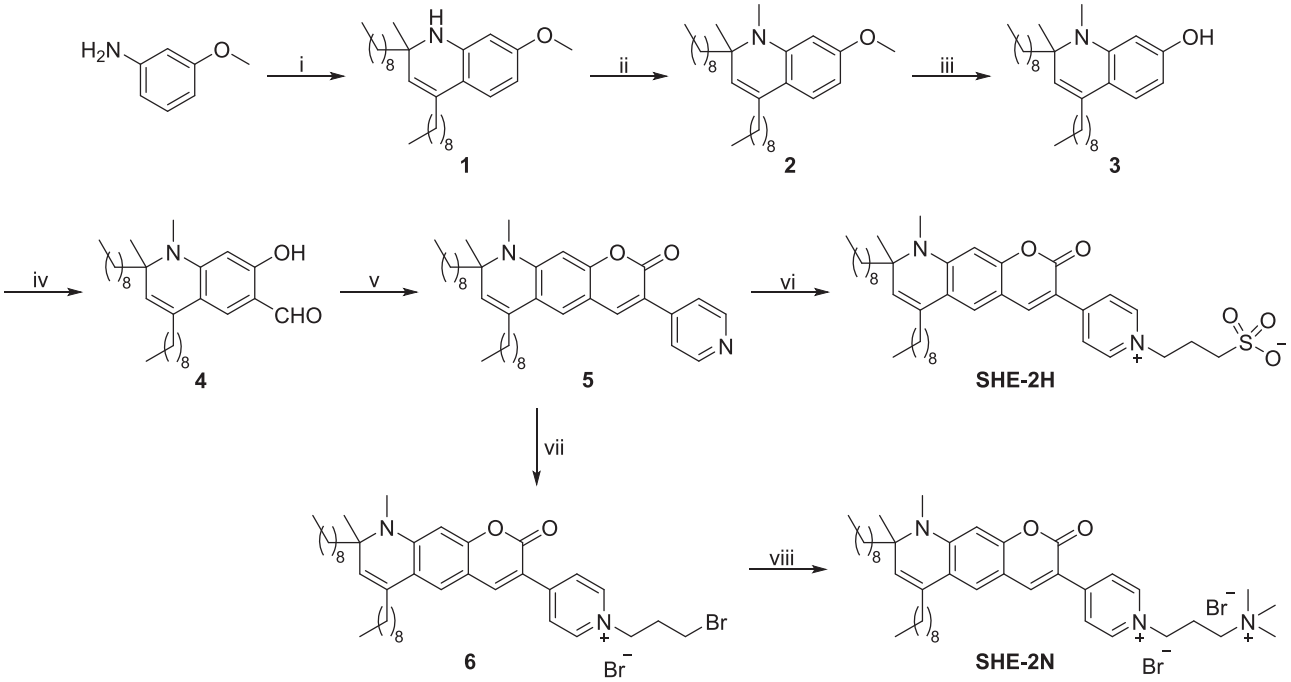

Scheme 1. Reagents and conditions: (i) 2-undecanone, $InCl_3$, 60 °C, 62%; (ii) MeI, K_2CO_3, DMF 110 °C, 58%; (iii) BBr_3, DCM, −80 °C, 46%; (iv) $POCl_3$, DMF, 75 °C, 24%; (v) ethyl 2-(pyridin-4-yl)acetate, morpholine, EtOH, reflux, 72%; (vi) 1,3-propanesultone, acetone, RT, 75%; (vii) 1,3-dibromopropan, 60 °C, 73%; (viii) NMe_3, EtOH, RT, 89%.

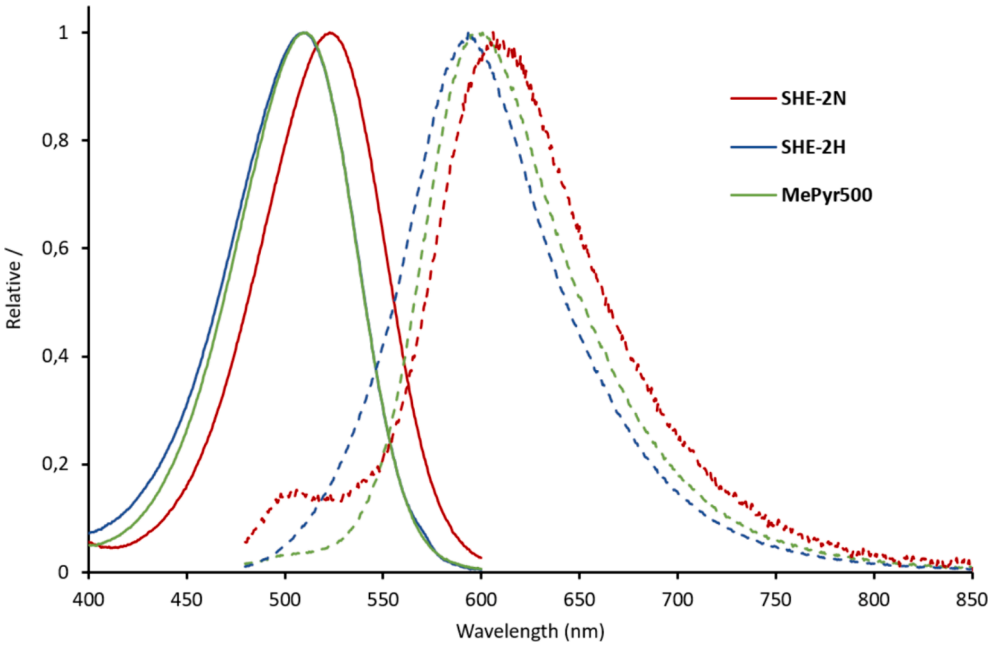

Fig. 2. Normalized absorption (solid line) and fluorescence emission (dashed line) spectra of probes **SHE-2H** (blue), **SHE-2N** (red) and **MePyr500** (green). Absorption spectra were recorded with 10^{-5} M solution in ethanol and fluorescence emission spectra were recorded with 10^{-6} M solutions in ethanol (λ_{ex} = 465 nm). (For interpretation of the references to colour in this figure legend, the reader is referred to the web version of this article.)

in terms of fluorescence signal from the membrane, as well as for possible morphology changes, which would indicate cytotoxicity of the tested probes.

Fluorescence microscopy of the probes revealed that the speed and distribution of cell labelling was remarkably different for all three probes (Fig. 3, top row). The quickest and most effective labelling was observed with **SHE-2N**, which labelled the cell membrane at a 10 μM concentration already in a few minutes. This probe was also the slowest to internalise into the cell. The original probe **MePyr500** was slower to label the cells, achieving a significant fluorescence signal on the cell membrane after 30 min at a 10 μM concentration, and labelled the internal cellular structures as well. According to all measured parameters, **SHE-2H** showed limited labelling efficiency: the probe did not label cells at a 10 μM concentration and labelled both the PM and the cell interior at higher concentration (50 μM, 30 min). The noticeable disparity in labelling effectiveness among the probes may be partially attributed to

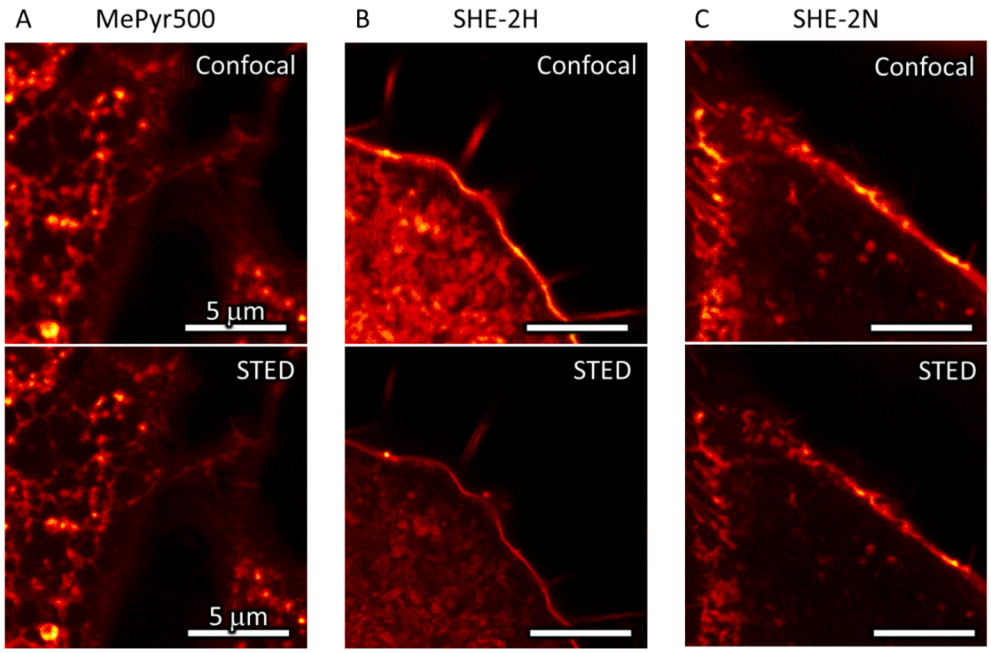

Fig. 3. Comparison of the resolution improvement of STED microscopy over confocal microscopy in living LA-4 cells, labelled with (A) **MePyr500** (10 µM, 60 min incubation), (B) **SHE-2H** (50 µM, 30 min incubation), and (C) **SHE-2N** (10 µM, 20 min incubation). The imaged area and pixel sizes are the same in all images; gating and laser powers were tuned to optimise the resolution improvement in STED images.

the significantly higher solubility of **SHE-2N** compared to **SHE-2H** and **MePyr500**. The solubility of **MePyr500**, **SHE-2H**, and **SHE-2N** in PBS buffer was determined to be 1.8 µM, 1.6 µM, and 470 µM, respectively. Additionally, the presence of negatively charged phosphate groups in the plasma membrane facilitates electrostatic interactions with positively charged groups on the probes, significantly improving the anchoring ability of the fluorophores[23].

Notably, the fluorescence of unbound probes in the surrounding aqueous medium (background) was negligible for all three probes, which allowed the imaging to be performed without washing away the unbound probes. This is especially important for 3D and time-lapse imaging, as it allows for a continuous exchange of the bleached probes on the cell structures with fresh fluorophores from the surrounding medium[24]. It also allows the labelling to be performed just prior imaging without exchanging the conditioned cell medium. In a noteworthy demonstration of the exceptional labelling specificity of **SHE-2N**, live cells were labelled with 1 µM of the probe and imaged intermittently for an uninterrupted duration of three days, underscoring the probe's robust performance[25].

2.4. Improvement of resolution with STED nanoscopy

In order to assess whether the designed probes exhibit increased resolution in STED microscopy, we compared the confocal and STED images of labelled LA-4 epithelial cells (Fig. 3). All three probes exhibited improved resolution in STED nanoscopy compared to the confocal image, despite the lengthening of the aliphatic chains and addition of a polar head group in the new probes.

2.5. Cytotoxicity

During live-cell imaging of **SHE-2H**, we observed unusual morphology of labelled cells observed at a 50 µM this concentration, which suggests that the probe is cytotoxic. At this concentration, long needle-like aggregates of the probe were also observed under bright-field illumination. The cytotoxicity assay on LA-4 cells confirmed the cytotoxic effect of **SHE-2H** at 50 µM (Fig. 4). Interestingly, **SHE-2N** is actually more cytotoxic than **SHE-2H** at the same probe concentration,

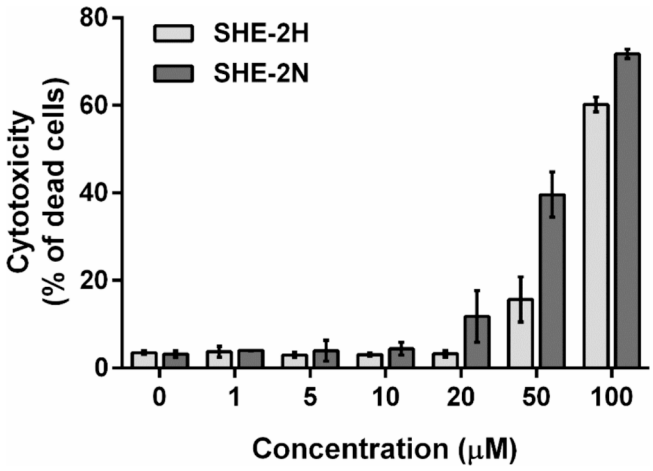

Fig. 4. *In vitro* cytotoxicity profile of compounds **SHE-2H** and **SHE-2N**. LA-4 cells were incubated in the presence of increasing concentrations of compounds (0–100 µM) in complete medium. After 24 h, the cytotoxicity was evaluated using SYTOTOX Blue dye and flow cytometry. Data indicates the percentages of dead cells and are means ± SD of two independent experiments, each performed in duplicate.

but is in the end more suitable for live-cell imaging than **SHE-2H**, as it requires significantly lower probe concentrations for sufficient labelling.

2.6. Two-photon excitation

We next tested the suitability of the probes for two-photon excitation (2PE) microscopy, which is usually used for superior sectioning capabilities due to focal-limited fluorescence excitation. Namely, as the cross-section for 2PE absorption strongly depends on the molecular structure of the probe, not all fluorescent probes exhibit noticeable florescence in 2PE microscopy. Because the 2PE excitation is the strongest at approximately double the wavelength (half the energy) of the wavelength used in one-photon excitation (1PE) microscopy[26], we

scanned the wavelength of 2PE excitation in the range between 800 nm and 1200 nm, and observed the corresponding fluorescence of labelled LA-4 cells. The 2PE excitation maximum of all three probes was at about 900 nm, and all probes exhibited strong fluorescence when excited with 37 mW average power in the sample plane. As is shown in the micrographs on Fig. 5, the signal in 2PE microscopy originates from the same structures as in 1PE microscopy, but with considerably decreased out-of-focus signal. This is best seen in the left-most column, where out-of-focus haze is present in the 1PE images (yellow arrows), but not in the corresponding 2PE images (white arrows). Also, the in-plane structures appear more defined and clearer in 2PE images due to focal limited excitation. To sum up, all three probes are suitable for 2PE microscopy, and could thus be used for imaging deep into scattering samples, e.g. biological tissues.

2.7. Photostability

Another crucial requirement for STED-compatible probes is high photostability in order to withstand the bleaching induced by powerful STED lasers. We estimated the photostability of the synthesized probes by continuously measuring a small field-of-view of labelled LA-4 cells for two minutes. As a benchmark for the comparison, commercially available probes CellMask Orange and STED-compatible STAR RED DPPE (a.k.a. KK114 DPPE) were measured as well. All probes were measured using the same imaging parameters to allow for a valid comparison. According to our measurements, all newly-synthesized probes exhibit exceptionally high photostability (Fig. 6), comparable to or even higher than STAR RED DPPE, and are therefore appropriate for continuous super-resolution live imaging of dynamic structures using STED microscopy. Of the tested probes, **MePyr500** and **SHE-2N** are the most photostable.

To better visualise the difference in photostability between **SHE-2N** and the commercially available STAR RED DPPE, we filmed a STED 3D stack of labelled LA-4 epithelial cells (Fig. 7). Due to its high photostability, **SHE-2N** enabled longer and more detailed 3D scans than STAR RED DPPE under the same imaging circumstances. Thus, **SHE-2N** excels also in applications where tracking of objects with high spatial resolution is needed.

2.8. Characterisation of *SHE-2N* in model membranes

Coumarin-based derivatives have been previously identified as environment-sensitive fluorophores[27,28]. The probe **SHE-2N** has several similarities to **Di-4-ANEPPDHQ**, a frequently used and STED-able polarity-sensitive probe[29]. Both are essentially pull–push dyes with electron-donating amine and electron-accepting pyridinium moiety.

To explore spectrophotometric characteristics of **SHE-2N** within the lipid environment, we analysed the spectral properties and the fluorescence lifetime of the probe in model membrane systems. For this purpose, we prepared giant unilamellar vesicles (GUVs) composed of pure POPC lipids (POPC 0% Chol) or of POPC in combination with cholesterol (1:1 M ratio; POPC 50% Chol) (Fig. 8A).

The emission spectra of the probe showed a slight red-shift of the average fluorescence peak maximum in the presence of cholesterol: the spectral peaks were at 576 nm and 582 nm for POPC 0% Chol and POPC 50% Chol, respectively (Fig. 8B-C). When analysing the probe lifetime in the lipid environment, we observed a shorter fluorescence lifetime of **SHE-2N** in POPC 50% Chol compared to POPC 0% Chol (tau1 2.3 ns and 2.8 ns, respectively) (Fig. 8D), consistent with the more red-shifted spectra of a polarity-sensitive probe[30,31]. Interestingly, however, the direction of shifts due to cholesterol content in POPCs was in the opposite direction than normally observed with polarity-sensitive probes[30,31]. Given that the spectrum in apolar membranes is blue-shifted compared to the more polar ethanol (compare Figs. 8 and 2), which corresponds to regular solvatochromicity, we hypothesise that the unconventional shift in membranes may originate in different vertical location of the dye in the membrane depending on the cholesterol content, which could be attributed to the rigidity of the probe. While the rigidity may preclude the use of this dye for polarity-probing applications, it ensures better brightness and excellent photostability[32,33], testified above (Figs. 6 and 7).

3. Conclusions

In summary, we have successfully designed, synthesized, and characterized two novel STED-able coumarin-based membrane probes,

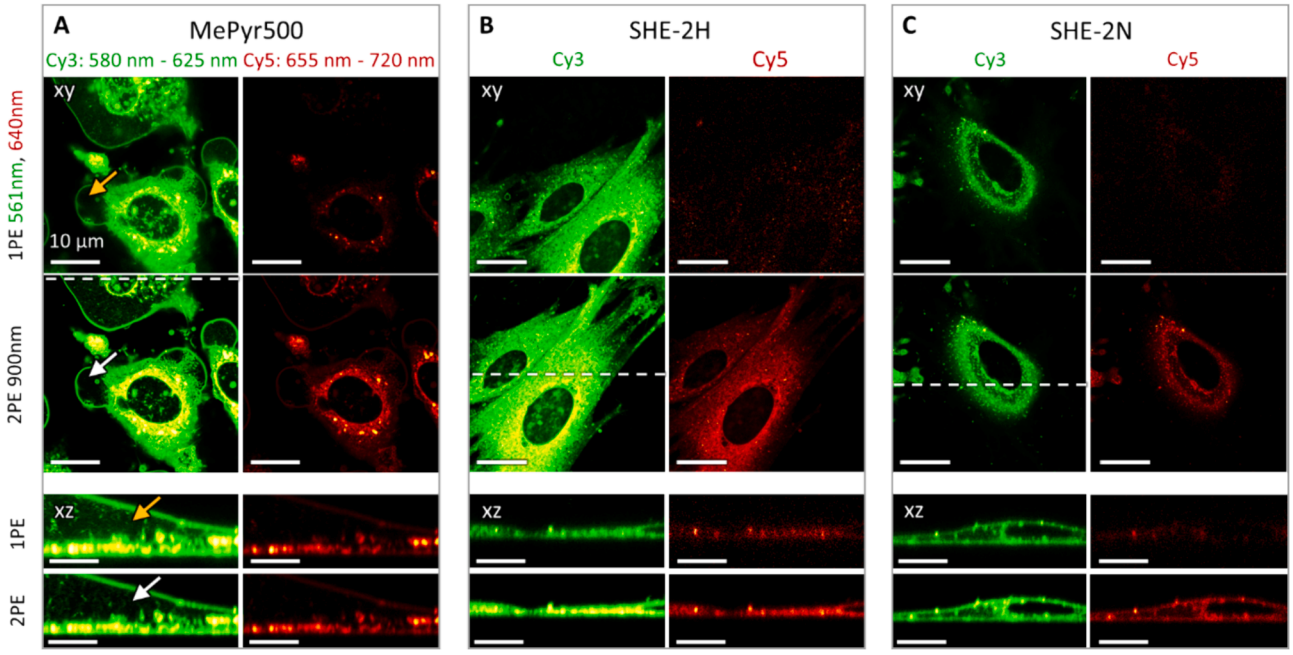

Fig. 5. Comparison of confocal (1PE) and 2PE micrographs (excited at optimal wavelengths) for all three probes on living LA-4 cells: (A) **MePyr500**, (B) **SHE-2H** and (C) **SHE-2N**. The imaged range, pixel sizes, 2PE wavelength and laser powers are the same in all images.

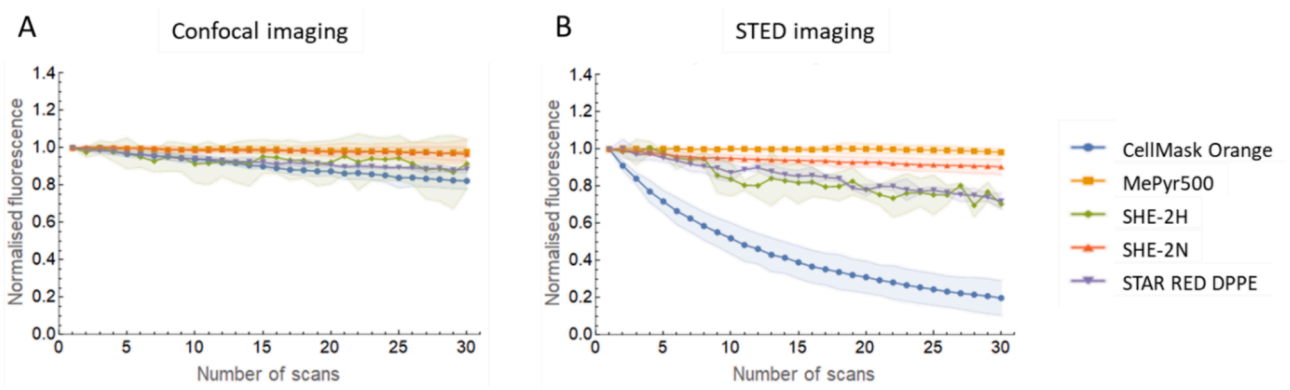

Fig. 6. Photostability of newly synthesized probes, compared to commercially available probes CellMask Orange and STED-dedicated STAR RED DPPE. The fluorescently labelled LA-4 cells were continuously imaged using either confocal (left) or STED microscopy (right) after washing the freely-floating probe from the sample and replacing it with fresh medium. All measurements were performed on the same day using identical imaging parameters. (For interpretation of the references to colour in this figure legend, the reader is referred to the web version of this article.)

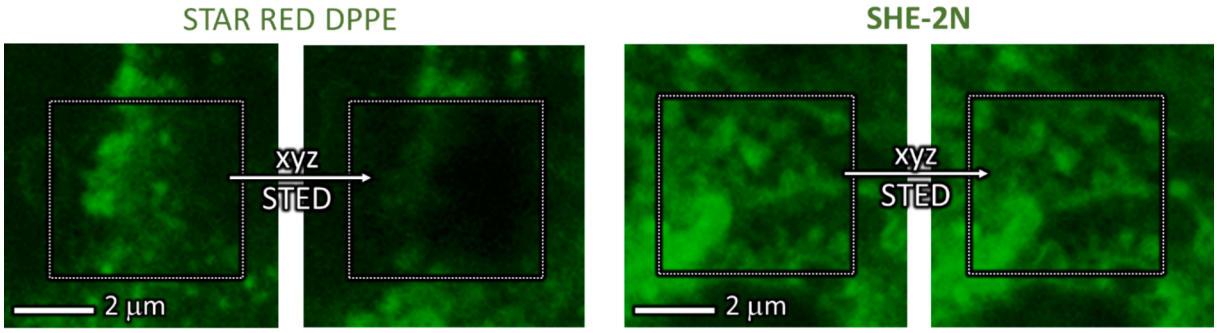

Fig. 7. Comparison of STED-induced photobleaching during 3D scanning for STAR RED DPPE (left) and **SHE-2N** (right) in live LA-4 cells. The imaging parameters were the same for both combinations of probes. (For interpretation of the references to colour in this figure legend, the reader is referred to the web version of this article.)

namely **SHE-2H** and **SHE-2N**. The straightforward synthesis procedures we employed render these probes readily accessible, holding great promise for widespread adoption in various research settings. Notably, **SHE-2N** demonstrates swift cell labelling, coupled with minimal redistribution to intracellular membranes. Furthermore, at the concentrations used for labelling, **SHE-2N** did not exhibit any noticeable toxicity, which was also confirmed by our cytotoxicity study. The excitation and emission spectra of both probes are well matched with a 561 nm excitation laser and 775 nm STED laser, making them compatible with many current STED nanoscopes. Moreover, the probes are well-suited for two-photon excitation microscopy. Their high photostability also enables the use of higher laser powers and/or longer lasting experiments without excessive photobleaching. Because the probe **SHE-2N** displays minimal sensitivity to environmental changes – the emission spectrum and fluorescence lifetime slightly changed in response to alterations in lipid composition within GUVs – we firmly believe that **SHE-2N** is an excellent probe for live-cell STED microscopy of PMs and great addition to the current toolkit of fluorescent membrane probes.

4. Experimental section

4.1. Synthesis

Materials and methods. List of chemicals used during the synthesis is provided in the Supplementary data. All reactions were performed under argon atmosphere, unless otherwise stated. Analytical TLC was performed on Merck silica gel (60 F_{254}) plates (0.25 mm) and visualized with ultraviolet light. ^{1}H and ^{13}C NMR spectra were recorded on a Bruker AVANCE III 400 MHz NMR spectrometer, utilizing $CDCl_3$ and methanol-d_4 as solvents, with chemical shifts referenced to TMS or the residual solvent peaks. Mass spectra were obtained using a Thermo Scientific Q Exactive Plus mass spectrometer. Fluorescence and absorption spectra were measured using a Perkin Elmer LS 55 fluorescence spectrophotometer and a Varian Cary 50 UV–Vis spectrophotometer, respectively.

7-Methoxy-2-methyl-2,4-dinonyl-1,2-dihydroquinoline (1). m-Anisidine (3.0 g, 24.4 mmol, 1 equiv), $InCl_3$ (300 mg, 1.36 mmol, 0.055 equiv) and 2-undecanone (15.1 mL, 17.1 mmol, 3 equiv) were stirred under an inert atmosphere at 60 °C for 24 h. 2-Undecanone was removed from reaction mixture by vacuum distillation. The crude product was purified by flash chromatography (EtOAc:hexane, 1:30), to give the desired product (62%) as light brown oil. ^{1}H NMR (400 MHz, $CDCl_3$) δ 6.98 (d, $J = 8.4$ Hz, 1H), 6.15 (dd, $J = 8.4$, 2.4 Hz, 1H), 5.99 (d, $J = 2.5$ Hz, 1H), 5.07 (s, 1H), 3.74 (s, 3H), 3.59 (bs, 1H), 2.38 – 2.24 (m, 2H), 1.62 – 1.10 (m, 33H), 0.92 – 0.83 (m, 6H). HRMS (ESI): *m/z* calcd for $C_{29}H_{50}NO$ $[M + H]^+$ 428.3880; found 428.3887.

7-Methoxy-1,2-dimethyl-2,4-dinonyl-1,2-dihydroquinoline (2). Compound **1** (6.4 g, 15 mmol, 1 equiv) was dissolved in DMF (35 mL). K_2CO_3 (3.1 g, 22.5 mmol, 1.5 equiv) and MeI (1.4 mL, 22.5 mmol, 1.5 equiv) were added and the reaction mixture was stirred at 110 °C for 15 h. Then the reaction mixture was cooled to room temperature, a mixture of methanol and 25% aqueous solution of ammonia (5 mL, 1:1 *v/v*) was added and the reaction mixture was stirred at room temperature for 30 min. EtOAc (150 mL) was then added to the reaction mixture and the solution was transferred to the separatory funnel. The solution was washed with water (5 × 100 mL), brine (1 × 50 mL) and dried over Na_2SO_4. The solvent was evaporated under reduced pressure and the crude product was purified by flash chromatography (EtOAc:hexane,

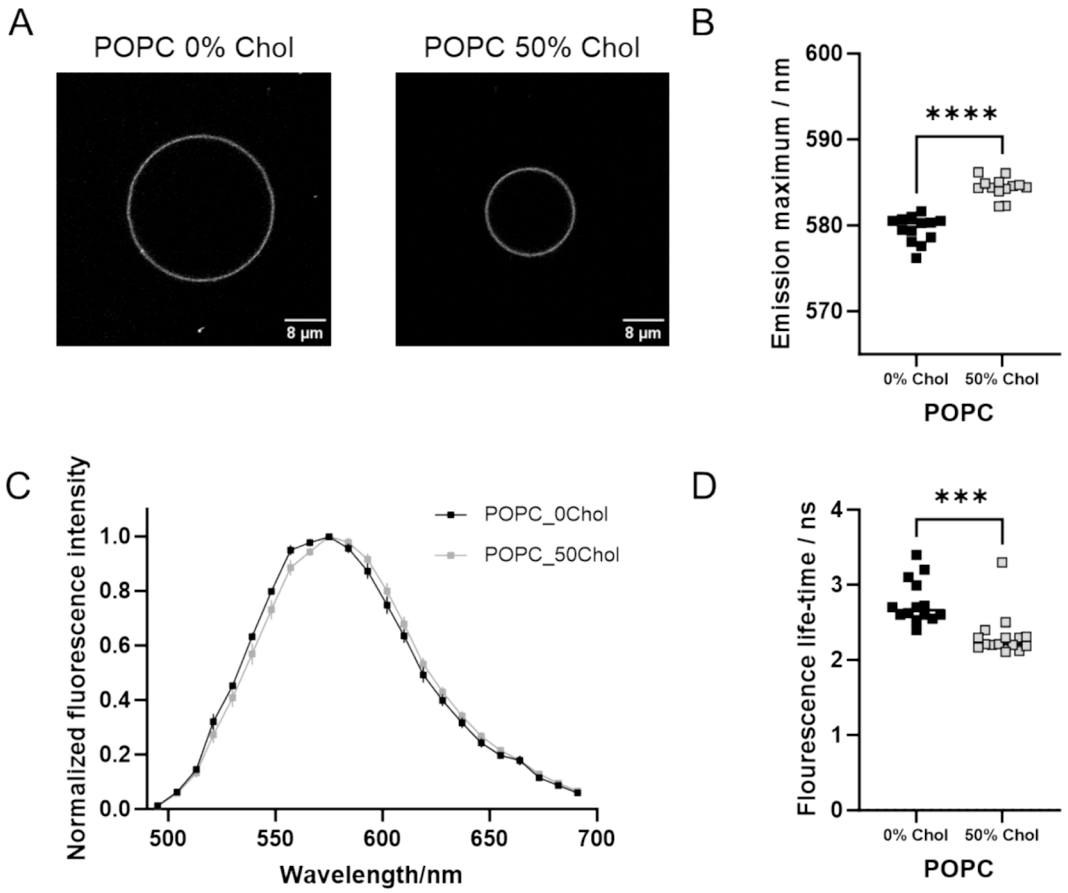

Fig. 8. Spectral and lifetime analysis of **SHE-2N** in giant unilamellar vesicles (GUVs). A) Representative GUVs with two different lipid compositions labelled with **SHE-2N**. B) Emission maximum of **SHE-2N** in GUVs containing POPC or POPC with 50% cholesterol. C) Fluoresce spectra of **SHE-2N** in GUVs with two different compositions. Excitation wavelength was 488 nm. D) Fluorescence lifetime of **SHE-2N** in GUVs. Each datapoint in B and D correspond to the average value obtained from a separate GUV. Statistical analysis was performed with the student *t*-test. ***$p < 0.001$, ****$p < 0.0001$.

1:50), to give the desired product (58%) as a light brown oil. ^{1}H NMR (400 MHz, $CDCl_3$) δ 6.96 (d, $J = 8.3$ Hz, 1H), 6.12 (dd, $J = 8.3$, 2.4 Hz, 1H), 6.04 (d, $J = 2.4$ Hz, 1H), 4.97 (s, 1H), 3.78 (s, 3H), 2.71 (s, 3H), 2.41 – 2.19 (m, 2H), 1.87 – 1.73 (m, 1H), 1.58 – 1.47 (m, 2H), 1.45 – 1.05 (m, 30H), 0.93 – 0.82 (m, 6H). HRMS (ESI): *m/z* calcd for $C_{30}H_{52}NO$ $[M + H]^+$ 442.4037; found 442.4043.

1,2-Dimethyl-2,4-dinonyl-1,2-dihydroquinolin-7-ol (**3**). Compound **2** (1.57 g, 3.66 mmol, 1 equiv) was dissolved in dry DCM (50 mL) and cooled to −80 °C. Solution of BBr_3 in DCM (10 mL, 10 mmol, 2.7 equiv) was added dropwise to the reaction mixture. The temperature of the reaction mixture was allowed to reach room temperature and the reaction mixture was stirred for further 4 h at room temperature. MeOH (20 mL) was added dropwise to the reaction mixture, followed by 10% aqueous solution of Na_2CO_3 (30 mL). pH of the aqueous phase was adjusted to 7, then the mixture was transferred to separatory funnel. Organic phase was washed with water (3 × 50 mL), brine (1 × 30 mL) and dried over Na_2SO_4. The solvent was evaporated under reduced pressure and the crude product was purified by flash chromatography (EtOAc:hexane, 1:6), to give the desired product (46%) as a light brown oil. ^{1}H NMR (400 MHz, $CDCl_3$) δ 6.89 (d, $J = 8.1$ Hz, 1H), 6.02 (dd, $J = 8.1$, 2.4 Hz, 1H), 5.98 (d, $J = 2.4$ Hz, 1H), 4.95 (s, 1H), 4.82 (s, 1H), 2.69 (s, 3H), 2.39 – 2.24 (m, 2H), 1.85 – 1.74 (m, 1H), 1.59 – 1.48 (m, 2H), 1.44 – 1.02 (m, 30H), 0.95 – 0.80 (m, 6H). ^{13}C NMR (101 MHz, $CDCl_3$) δ 156.36, 147.80, 132.66, 125.06, 124.04, 115.33, 101.55, 97.52, 59.71, 41.65, 32.23, 32.07, 32.05, 30.60, 30.16, 29.82, 29.77, 29.71, 29.51, 29.47, 28.53, 27.32, 24.94, 22.83, 14.25. HRMS (ESI): *m/z* calcd for $C_{29}H_{50}NO$ $[M + H]^+$ 428.3887; found 428.3882.

7-Hydroxy-1,2-dimethyl-2,4-dinonyl-1,2-dihydroquinoline-6-carbaldehyde (**4**). $POCl_3$ (1.53 mL, 16.4 mmol, 10 equiv) was added dropwise to DMF (7 mL) cooled on an ice bath and the solution was stirred at room temperature for 30 min. Phenol **3** (700 mg, 1.64 mmol, 1 equiv) dissolved in DMF (7 mL) was then added dropwise, and the mixture was stirred for 1.5 h at 75 °C. The reaction mixture was diluted with EtOAc (100 mL), and 5% Na_2CO_3 (10 mL) was added. pH of the aqueous phase was adjusted to 7 with 5% Na_2CO_3, and the mixture was then transferred to separatory funnel. The organic phase was washed with water (5 × 30 mL), brine (1 × 30 mL) and dried over Na_2SO_4. The solvent was evaporated under reduced pressure and the crude product was purified by flash chromatography (EtOAc:hexane, 1:9), to give the desired product (24%) as a light brown oil. ^{1}H NMR (400 MHz, $CDCl_3$) δ 11.85 (s, 1H), 9.46 (s, 1H), 7.02 (s, 1H), 5.92 (s, 1H), 5.03 (s, 1H), 2.82 (s, 3H), 2.41 – 2.23 (m, 2H), 1.89 – 1.75 (m, 1H), 1.55 – 1.50 (m, 2H), 1.46 – 1.15 (m, 29H), 1.12 – 1.00 (m, 1H), 0.93 – 0.82 (m, 6H). ^{13}C NMR (101 MHz, $CDCl_3$) δ 191.70, 164.74, 153.14, 131.34, 127.13, 125.04, 114.47, 110.54, 95.44, 61.08, 41.82, 31.88, 31.83, 31.65, 31.34, 29.65, 29.62, 29.55, 29.53, 29.50, 29.31, 29.25, 28.93, 27.95, 24.49, 22.65, 22.63, 14.09, 14.07. HRMS (ESI): *m/z* calcd for $C_{30}H_{50}NO_2$ $[M + H]^+$ 456.3836; found 456.3827.

8,9-Dimethyl-6,8-dinonyl-3-(pyridin-4-yl)-8,9-dihydro-2*H*-pyrano [3,2-*g*] quinolin-2-one (**5**). Salicylaldehyde **4** (151 mg, 0.55 mmol, 1 equiv), ethyl 2-(pyridin-4-yl)acetate (126 µL, 0.83 mmol, 1.5 equiv), and morpholine (47 µL, 0.55 mmol, 1 equiv) were dissolved in anhydrous ethanol (20 mL). The reaction mixture was then refluxed for 15 h. After completion, the mixture was then cooled to room temperature, diluted with EtOAc (100 mL), and washed with 5% aqueous solution of citric acid (4 × 30 mL), water (4 × 30 mL), brine (1 × 30 mL) and dried

over Na_2SO_4. The solvent was evaporated under reduced pressure and the crude product was purified by flash chromatography (EtOAc:hexane, 1:1), to give the desired product (72%) as an orange solid. ^{1}H NMR (400 MHz, $CDCl_3$) δ 8.74 – 8.52 (m, 2H), 7.86 (s, 1H), 7.80 – 7.66 (m, 2H), 7.11 (s, 1H), 6.33 (s, 1H), 5.17 (s, 1H), 2.84 (s, 3H), 2.47 – 2.28 (m, 2H), 1.93 – 1.79 (m, 1H), 1.64 – 1.50 (m, 2H), 1.49 – 1.18 (m, 29H), 1.16 – 1.05 (m, 1H), 0.96 – 0.78 (m, 6H). ^{13}C NMR (101 MHz, $CDCl_3$) δ 160.88, 156.88, 150.76, 149.42, 144.02, 142.33, 131.44, 128.01, 122.45, 122.03, 119.31, 116.56, 108.58, 95.67, 61.18, 42.05, 32.04, 31.99, 31.47, 29.83, 29.79, 29.68, 29.48, 29.40, 29.00, 28.14, 24.78, 22.82, 14.23. HRMS (ESI): *m/z* calcd for $C_{37}H_{53}N_2O_2$ $[M + H]^+$ 557.4102; found 557.4103.

3-(4-(8,9-Dimethyl-6,8-dinonyl-2-oxo-8,9-dihydro-2*H*-pyrano [3,2-*g*] quinolin-3-yl)pyridin-1-ium-1-yl)propane-1-sulfonate (SHE-2H). Compound **5** (124 mg, 0.22 mmol, 1 equiv) was dissolved in acetone (30 mL). 1,3-Propanesultone (70 mg, 0.54 mmol, 2.6 equiv) was added to this solution, and the reaction mixture was stirred at room temperature for 2 days. After completion, confirmed by TLC, solvent was removed under reduced pressure and the residue was triturated with diethyl ether (2 × 20 mL) and hexane (4 × 20 mL). Crude product was purified by flash chromatography (DCM:MeOH, 9:1 to 5:1, ammonia gas was bubbled through mobile phase prior its use), to give the desired product (75%) as a red solid. ^{1}H NMR (400 MHz, MeOD) δ 8.83 – 8.78 (m, 2H), 8.65 (s, 1H), 8.61 – 8.56 (m, 2H), 7.35 (s, 1H), 6.40 (s, 1H), 5.34 (s, 1H), 4.73 (t, J = 7.2 Hz, 2H), 2.96 (s, 3H), 2.89 (t, J = 6.9 Hz, 2H), 2.56 – 2.32 (m, 4H), 2.03 – 1.92 (m, 1H), 1.66 – 1.54 (m, 2H), 1.48 – 1.19 (m, 29H), 1.16 – 1.06 (m, 1H), 0.93 – 0.81 (m, 6H). ^{13}C NMR (101 MHz, MeOD) δ 161.48, 159.67, 154.51, 153.69, 147.67, 144.66, 132.37, 129.98, 125.03, 124.77, 121.18, 110.84, 110.42, 96.13, 63.32, 59.85, 48.25, 42.58, 33.11, 33.05, 32.78, 32.45, 30.84, 30.74, 30.72, 30.60, 30.49, 30.40, 29.32, 29.20, 28.12, 25.86, 23.75, 23.72, 14.46. HRMS (ESI): *m/z* calcd for $C_{40}H_{59}N_2O_5S$ $[M + H]^+$ 679.4139; found 679.4134.

1-(3-Bromopropyl)-4-(8,9-dimethyl-6,8-dinonyl-2-oxo-8,9-dihydro-2*H*-pyrano [3,2-*g*] quinolin-3-yl)pyridin-1-ium bromide (6). Compound **5** (145 mg, 0.26 mmol, 1 equiv) was dissolved in 1,3-dibromopropane (132 μL, 1.3 mmol, 5 equiv) and the reaction mixture was stirred at 60 °C for 4 h. After completion, the crude product was purified by flash chromatography (DCM:MeOH, from 20:1 to 10:1), to give the desired product (73%) as red viscous oil. ^{1}H NMR (400 MHz, $CDCl_3$) δ 9.23 – 9.18 (m, 2H), 8.74 – 8.69 (m, 2H), 8.65 (s, 1H), 7.38 (s, 1H), 6.31 (s, 1H), 5.22 (s, 1H), 5.01 (t, J = 7.0 Hz, 2H), 3.54 (t, J = 6.1 Hz, 2H), 2.92 (s, 3H), 2.77 – 2.65 (m, 2H), 1.95 – 1.82 (m, 1H), 1.64 – 1.51 (m, 2H), 1.44 – 1.14 (m, 29H), 1.12 – 1.00 (m, 1H), 0.92 – 0.80 (m, 6H). ^{13}C NMR (101 MHz, $CDCl_3$) δ 160.00, 158.56, 153.24, 152.50, 146.37, 143.61, 131.42, 128.11, 124.21, 123.88, 120.27, 109.38, 109.16, 95.27, 62.13, 58.57, 41.95, 33.84, 31.99, 31.97, 31.92, 31.77, 29.75, 29.69, 29.63, 29.60, 29.44, 29.34, 29.22, 29.09, 27.91, 24.66, 22.77, 22.74, 14.21, 14.18. HRMS (ESI): *m/z* calcd for $C_{40}H_{58}N_2O_2Br$ $[M]^+$ 677.3676; found 677.3671.

4-(8,9-Dimethyl-6,8-dinonyl-2-oxo-8,9-dihydro-2*H*-pyrano [3,2-*g*] quinolin-3-yl)-1-(3-(trimethylammonio)propyl)pyridin-1-ium dibromide (SHE-2N). Bromide **6** (130 mg, 0.19 mmol, 1 equiv) was dissolved in 4.2 M trimethylamine solution in ethanol (5 mL) and stirred at room temperature for 24 h. Following this, solvents were removed under reduced pressure and the residue was triturated with diethyl ether (2 × 20 mL) and hexane (4 × 20 mL). The crude product was purified by flash chromatography (DCM:MeOH:H_2O, 24:8:1, ammonia gas was bubbled through mobile phase prior its use), to give the desired product (89%) as a red solid. ^{1}H NMR (400 MHz, MeOD) δ 9.03 – 8.94 (m, 2H), 8.71 (s, 1H), 8.66 – 8.58 (m, 2H), 7.34 (s, 1H), 6.33 (s, 1H), 5.29 (s, 1H), 4.73 (t, J = 7.3 Hz, 2H), 3.75 – 3.63 (m, 2H), 3.28 (s, 9H), 2.95 (s, 3H), 2.73 – 2.61 (m, 2H), 2.49 – 2.27 (m, 1H), 2.35 – 2.22 (m, 1H), 2.02 – 1.99 (m, 1H), 1.64 – 1.50 (m, 2H), 1.44 (s, 3H), 1.41 – 1.15 (m, 26H), 1.14 – 1.01 (m, 1H), 0.92 – 0.79 (m, 6H). ^{13}C NMR (101 MHz, MeOD) δ 161.26, 159.53, 154.40, 153.61, 147.77, 144.69, 132.31, 129.75, 125.00, 124.89, 121.09, 110.45, 110.41, 96.11, 63.83, 63.29, 57.84, 54.03, 42.60, 33.09, 33.03, 32.71, 32.63, 30.86, 30.78, 30.75, 30.71, 30.63, 30.62, 30.50, 30.41, 29.45, 29.13, 26.19, 25.84, 23.74, 23.71, 14.55, 14.54. HRMS (ESI): *m/z* calcd for $C_{43}H_{67}N_3O_2$ $[M]^{2+}$ 328.7611; found 328.7610.

4.2. Cytotoxicity assay

The toxic profile of compounds was determined with high-affinity nucleic acid fluorescence dye SYTOTOX Blue assessed by flow cytometry. LA-4 cells were seeded in 12-well culture plates (5 × 104/well) and next day treated with increasing concentrations of compounds **SHE-2H** and **SHE-2N**. After 24 h treatment, cells were harvested and washed in cold phosphate-buffered saline (PBS), and labelled with SYTOTOX Blue dye (1 μM; Thermo Fisher Scientific) for 15 min at room temperature. Cells were then analysed for cytotoxicity by flow cytometry on Attune NxT flow cytometer (Thermo Fisher Scientific). The percentage of dead cells was evaluated using FlowJo software (FlowJo, LLC, Ashland, OR, USA).

4.3. Imaging

4.3.1. Preparation of giant unilamellar vesicle (GUVs)

GUVs were prepared using electroformation method as previously described.[34] Briefly, 1-palmitoyl-2-oleoyl-*sn-glycero*-3-phosphocholine (POPC) without or with cholesterol (50 mol%) was diluted in chloroform at the concentration of 1 mg/mL. 5 μL of each solution were applied and dried out onto two parallel platinum wires mounted on a cap of custom-built GUV Teflon chamber to obtain lipid film. The GUVs were formed in 300 mM sucrose solution at room temperature by applying an alternating electric current of 10 Hz and 2 V to the wires for an hour followed by the decrease of the frequency to 2 Hz for 30 min. 100 μL of GUV suspensions were then labelled with **SHE-2N** in the final concentration of 20 μM. Labelled samples were diluted in 250 μL PBS and imaged in BSA-pre-coated 8-well plastic-bottom Ibidi chambers (#1.5).

4.3.2. Confocal spectral imaging

Equatorial planes of the GUVs stained with **SHE-2N** were imaged with a 40 × water immersion objective (NA = 1.1) on Zeiss LSM 780 confocal microscope equipped with a 32-channel GaAsP detector array as described before.[35] Laser light at 488 nm was selected for fluorescence excitation of **SHE-2N**. Fluorescence spectra were acquired between 495 and 691 nm in 8.9-nm intervals. The spectral series of images were saved in the.lsm format and then analysed using Fiji/ImageJ and a custom spectral fitting software written in Mathematica.[36].

4.3.3. Fluorescence life-time imaging

FLIM measurements were performed with a Leica TCS SP8 (Leica Microsystems) inverted confocal microscope with an 86 × water immersion objective (NA = 1.2). The microscope was equipped with a time-correlated single-photon-counting module from PicoQuant. For excitation, the 488-nm line was selected from the pulsed white-light laser. The emitted photons were collected within the 575–625 nm spectral window using the internal hybrid detector in the photon-counting mode. At least 100 counts per pixel were collected in all cases. The fluorescence decay histograms from the selected regions with the membrane signal were fitted with a bi-exponential model using SymPhoTime 64 software (PicoQuant). The fitted fluorescence lifetime values of the slow component (tau1) were expressed as means ± standard deviation in ns.

4.3.4. Preparation of cells and probes for imaging

We tested the labelling efficiency, STED-ability and label distribution in the murine epithelial lung cell line LA-4 (ATCC CCL-196). The cells were cultured in accordance with ATCC guidelines: they were grown in full cell medium, consisting of Ham's F-12 K medium (ATCC),

complemented with 15% FCS (ATCC), 1% P/S (Sigma), and 1% NEAA (Gibco) and kept in a humid atmosphere in an incubator at 37 °C and 5 % CO_2 levels. A few days prior to imaging, they were seeded into 8-well μμ-slides (Ibidi) with a 1.5H glass bottom and further grown in cell medium as before.

The probes were diluted from a 10 mM stock in DMSO to a 10 μM concentration in Live Cell Imaging Solution (LCIS, Molecular probes) just prior to labelling the cells in order to minimize probe aggregation. After cell medium was removed from the cells, they were incubated with 200 μL of diluted probe per well and imaged after the cells have been appropriately stained. Except where noted otherwise, the cells remained incubated with the probe during imaging. During the incubation, cells were constantly being monitored both in terms of the fluorescence signal from the membrane, as well as for possible morphology changes, indicating cytotoxicity of the tested probes. The final concentration of probes used for the photo-physical characterisation on cells was 10 μM for **SHE-2N** and **MePyr500**, 50 μM for **SHE-2H**, 2 μg/mL for CellMask Orange, and 1 μM for STAR RED DPPE.

4.3.5. Confocal, stimulated emission depletion (STED) and two-photon excitation (2PE) imaging

Imaging of the samples was performed on an Olympus IX83 microscope with a 60 × water-immersion objective (NA 1.2), custom-upgraded by Abberior Instruments with 561 nm and 640 nm excitation lasers (120 ps pulse length, 50 μW mean power), a 775 nm STED laser (1.2 ns pulse length, 170 mW mean power), and two avalanche photodiodes for fluorescence detection in ranges 580–625 nm and 655–720 nm, as defined by pre-filters and a dichroic. All imaging was performed at 80 MHz frequency and with a 1.1 A.U. pinhole, except where noted otherwise.

For the comparison of the resolution between confocal and STED microscopy, a field of view of 15 μm × 15 μm was imaged with a 30 nm pixel size. The dwell time was 10 μs for confocal and 30 μs for STED microscopy, and the pinhole size was 0.6 AU. Other parameters (gating, laser powers) were tuned for each probe separately to achieve the best possible resolution.

For comparison of 2PE and confocal imaging, a high-power Chameleon Discovery laser was also used for imaging, using 900 nm wavelength, 37 mW power in the sample plane, and pulse lengths of 100 fs. An 80 μm × 80 μm field of view, 10 μs dwell-time, and 100 nm pixel size were chosen for imaging.

The photostability of probes was determined by measuring 3 × 30 consecutive images with a 10 μm × 10 μm field of view, 50 nm large pixels and a 10 μs dwell-time per pixel. The sample was excited with 13 μW laser power and, in the case of 2D STED-induced bleaching, depleted using an 80 mW STED laser.

For the comparison of STED-induced photobleaching of STAR RED DPPE and **SHE-2N**, cells were labelled either with 10 μM **SHE-2N** or 1 μM STAR RED DPPE in LCIS. Cell remained in this medium throughout the imaging. For the measurement, the sample was excited using 10 μW 561 nm and 640 nm excitation lasers and depleted using a 35 mW 775 nm STED laser. The dwell time for each pixel was 20 μs. The 3D measurements (xyz) consisted of a 5 μm × 5 μm × 5 μm cube with 100 × 100 × 50 pixels.

The data was acquired using Imspector 16.3.10630 software. The laser powers in the sample plane were determined by measuring the power at the objective back focal plane, passing the light through a manual shutter closed to the size of the objective back aperture and then focusing to a Thorlabs Power Meter S120C.

CRediT authorship contribution statement

Hana Kokot: Writing – review & editing, Writing – original draft, Visualization, Investigation, Conceptualization. **Boštjan Kokot:** Writing – review & editing, Writing – original draft, Visualization, Investigation, Conceptualization. **Anja Pišlar:** Writing – review & editing, Visualization, Investigation. **Hana Esih:** Writing – review & editing, Writing – original draft, Visualization, Investigation, Conceptualization. **Alen Gabrič:** Investigation. **Dunja Urbančič:** Writing – review & editing, Writing – original draft, Visualization, Investigation, Conceptualization. **Rojbin El:** Writing – review & editing, Investigation, Conceptualization. **Iztok Urbančič:** Writing – review & editing, Writing – original draft, Supervision, Investigation, Funding acquisition, Conceptualization. **Stane Pajk:** Writing – review & editing, Writing – original draft, Visualization, Supervision, Funding acquisition, Conceptualization.

Declaration of competing interest

The authors declare that they have no known competing financial interests or personal relationships that could have appeared to influence the work reported in this paper.

Acknowledgments

This work was supported by the Slovenian Research and Innovation Agency (core research funding P1-0208 and P1-0060 and projects J3-3079, J7-2596, N1-0240), Ministry of Higher Education, Science and Innovation, Slovenia; the European Regional Development Fund (OP20.05187 RI-SI-EATRIS), EU; and Marie Skłodowska-Curie Fellowship (707348). We thank the Wolfson Imaging Centre (University of Oxford), United Kingdom, for access to the microscopes. We also thank Megi Tinev for her help with some of the additional experiments and analysis.

Appendix A. Supplementary data

Supplementary data to this article can be found online at https://doi.org/10.1016/j.bioorg.2024.107554.

References

[1] C. Dias, J. Nylandsted, Plasma membrane integrity in health and disease: significance and therapeutic potential, Cell Discov. 7 (2021) 4, https://doi.org/10.1038/s41421-020-00233-2.
[2] E. Alizadeh, J. Castle, A. Quirk, C.D.L. Taylor, W. Xu, A. Prasad, Cellular morphological features are predictive markers of cancer cell state, Comput. Biol. Med. 126 (2020) 104044, https://doi.org/10.1016/j.compbiomed.2020.104044.
[3] S.J. Sahl, S.W. Hell, S. Jakobs, Fluorescence nanoscopy in cell biology, Nat. Rev. Mol. Cell Biol. 18 (2017) 685–701, https://doi.org/10.1038/nrm.2017.71.
[4] J. Valli, A. Garcia-Burgos, L.M. Rooney, B. Vale De Melo E Oliveira, R.R. Duncan, C. Rickman, Seeing beyond the limit: A guide to choosing the right super-resolution microscopy technique, J. Biol. Chem. 297 (2021) 100791, https://doi.org/10.1016/j.jbc.2021.100791.
[5] S.W. Hell, J. Wichmann, Breaking the diffraction resolution limit by stimulated emission: stimulated-emission-depletion fluorescence microscopy, Opt. Lett. 19 (1994) 780, https://doi.org/10.1364/OL.19.000780.
[6] E. Sezgin, F. Schneider, S. Galiani, I. Urbančič, D. Waithe, B.C. Lagerholm, C. Eggeling, Measuring nanoscale diffusion dynamics in cellular membranes with super-resolution STED–FCS, Nat. Protoc. (2019), https://doi.org/10.1038/s41596-019-0127-9.
[7] K. Svoboda, R. Yasuda, Principles of Two-Photon Excitation Microscopy and Its Applications to Neuroscience, Neuron 50 (2006) 823–839, https://doi.org/10.1016/j.neuron.2006.05.019.
[8] P.L. Appleton, A.J. Quyn, S. Swift, I. Näthke, Preparation of wholemount mouse intestine for high-resolution three-dimensional imaging using two-photon microscopy, J. Microsc. 234 (2009) 196–204, https://doi.org/10.1111/j.1365-2818.2009.03163.x.
[9] F. Helmchen, W. Denk, Deep tissue two-photon microscopy, Nat. Methods 2 (2005) 932–940, https://doi.org/10.1038/nmeth818.
[10] X. Duan, M. Zhang, Y.-H. Zhang, Organic fluorescent probes for live-cell super-resolution imaging, Front. Optoelectron. 16 (2023) 34, https://doi.org/10.1007/s12200-023-00090-3.
[11] S. Jeong, J. Widengren, J.-C. Lee, Fluorescent Probes for STED Optical Nanoscopy, Nanomater. 12 (2021) 21, https://doi.org/10.3390/nano12010021.
[12] G. Vicidomini, P. Bianchini, A. Diaspro, STED super-resolved microscopy, Nat Methods 15 (2018) 173–182, https://doi.org/10.1038/nmeth.4593.
[13] M. Albota, D. Beljonne, J.-L. Brédas, J.E. Ehrlich, J.-Y. Fu, A.A. Heikal, S.E. Hess, T. Kogej, M.D. Levin, S.R. Marder, D. McCord-Maughon, J.W. Perry, H. Röckel, M. Rumi, G. Subramaniam, W.W. Webb, X.-L. Wu, C. Xu, Design of Organic Molecules with Large Two-Photon Absorption Cross Sections, Science 281 (1998) 1653–1656, https://doi.org/10.1126/science.281.5383.1653.

[14] M. Collot, S. Pfister, A.S. Klymchenko, Advanced functional fluorescent probes for cell plasma membranes, Curr. Chem. Biol. 69 (2022) 102161, https://doi.org/10.1016/j.cbpa.2022.102161.
[15] J. Chen, T. Liu, J. Gao, L. Gao, L. Zhou, M. Cai, Y. Shi, W. Xiong, J. Jiang, T. Tong, H. Wang, Variation in Carbohydrates between Cancer and Normal Cell Membranes Revealed by Super-Resolution Fluorescence Imaging, Adv. Sci. 3 (2016) 1600270, https://doi.org/10.1002/advs.201600270.
[16] H.-R. Jia, H.-Y. Wang, Z.-W. Yu, Z. Chen, F.-G. Wu, Long-Time Plasma Membrane Imaging Based on a Two-Step Synergistic Cell Surface Modification Strategy, Bioconjugate Chem. 27 (2016) 782–789, https://doi.org/10.1021/acs.bioconjchem.6b00003.
[17] X. Chen, X. Zhang, H.-Y. Wang, Z. Chen, F.-G. Wu, Subcellular Fate of a Fluorescent Cholesterol-Poly(ethylene glycol) Conjugate: An Excellent Plasma Membrane Imaging Reagent, Langmuir 32 (2016) 10126–10135, https://doi.org/10.1021/acs.langmuir.6b02288.
[18] T. Heek, J. Nikolaus, R. Schwarzer, C. Fasting, P. Welker, K. Licha, A. Herrmann, R. Haag, An Amphiphilic Perylene Imido Diester for Selective Cellular Imaging, Bioconjugate Chem. 24 (2013) 153–158, https://doi.org/10.1021/bc3005655.
[19] M. Collot, P. Ashokkumar, H. Anton, E. Boutant, O. Faklaris, T. Galli, Y. Mély, L. Danglot, A.S. Klymchenko, MemBright: A Family of Fluorescent Membrane Probes for Advanced Cellular Imaging and Neuroscience, Cell, Chem. Biol. 26 (2019) 600–614.e7, https://doi.org/10.1016/j.chembiol.2019.01.009.
[20] M. Collot, R. Kreder, A.L. Tatarets, L.D. Patsenker, Y. Mely, A.S. Klymchenko, Bright fluorogenic squaraines with tuned cell entry for selective imaging of plasma membrane vs. endoplasmic reticulum, Chem. Commun. 51 (2015) 17136–17139, https://doi.org/10.1039/C5CC06094J.
[21] S. Pajk, H. Majaron, M. Novak, B. Kokot, J. Štrancar, New coumarin- and phenoxazine-based fluorescent probes for live-cell STED nanoscopy, Eur. Biophys. J. 48 (2019) 485–490, https://doi.org/10.1007/s00249-019-01354-7.
[22] R. Giri, Fluorescence quenching of coumarins by halide ions, SAA 60 (2004) 757–763, https://doi.org/10.1016/S1386-1425(03)00287-7.
[23] L. Yang, Q. Chen, Z. Wang, H. Zhang, H. Sun, Small-molecule fluorescent probes for plasma membrane staining: Design, mechanisms and biological applications, Coordination Chem. Rev. 474 (2023) 214862, https://doi.org/10.1016/j.ccr.2022.214862.
[24] C. Spahn, J.B. Grimm, L.D. Lavis, M. Lampe, M. Heilemann, Whole-Cell, 3D, and Multicolor STED Imaging with Exchangeable Fluorophores, Nano Lett. 19 (2019) 500–505, https://doi.org/10.1021/acs.nanolett.8b04385.
[25] H. Kokot, B. Kokot, A. Sebastijanović, C. Voss, R. Podlipec, P. Zawilska, T. Berthing, C. Ballester-López, P.H. Danielsen, C. Contini, M. Ivanov, A. Krišelj, P. Čotar, Q. Zhou, J. Ponti, V. Zhernovkov, M. Schneemilch, Z. Doumandji, M. Pušnik, P. Umek, S. Pajk, O. Joubert, O. Schmid, I. Urbančič, M. Irmler, J. Beckers, V. Lobaskin, S. Halappanavar, N. Quirke, A.P. Lyubartsev, U. Vogel, T. Koklič, T. Stoeger, J. Štrancar, Prediction of Chronic Inflammation for Inhaled Particles: the Impact of Material Cycling and Quarantining in the Lung Epithelium, Adv. Mater. 32 (2020) 2003913, https://doi.org/10.1002/adma.202003913.
[26] R.K.P. Benninger, D.W. Piston, Two-Photon Excitation Microscopy for the Study of Living Cells and Tissues, CP Cell Biology 59 (2013), https://doi.org/10.1002/0471143030.cb0411s59.
[27] S. Pajk, M. Garvas, J. Štrancar, Fluorescent Membrane Probes Based on a Coumarin-Thiazole Scaffold, Acsi 66 (2019) 668–674, https://doi.org/10.17344/acsi.2019.5089.
[28] G. Signore, R. Nifosì, L. Albertazzi, B. Storti, R. Bizzarri, Polarity-Sensitive Coumarins Tailored to Live Cell Imaging, J. Am. Chem. Soc. 132 (2010) 1276–1288, https://doi.org/10.1021/ja9050444.
[29] L. Jin, A.C. Millard, J.P. Wuskell, H.A. Clark, L.M. Loew, Cholesterol-Enriched Lipid Domains Can Be Visualized by di-4-ANEPPDHQ with Linear and Nonlinear Optics, Biophys. J. 89 (2005) L04–L06, https://doi.org/10.1529/biophysj.105.064816.
[30] Y. Ma, A. Benda, J. Kwiatek, D.M. Owen, K. Gaus, Time-Resolved Laurdan Fluorescence Reveals Insights into Membrane Viscosity and Hydration Levels, Biophys. J. 115 (2018) 1498–1508, https://doi.org/10.1016/j.bpj.2018.08.041.
[31] F. Ragaller, E. Sjule, Y.B. Urem, J. Schlegel, R. El, D. Urbancic, I. Urbancic, H. Blom, E. Sezgin, Quantifying Fluorescence Lifetime Responsiveness of Environment-Sensitive Probes for Membrane Fluidity Measurements, J. Phys. Chem. B (2024) acs.jpcb.3c07006. Doi: 10.1021/acs.jpcb.3c07006.
[32] Y. Niko, A.S. Klymchenko, Emerging solvatochromic push–pull dyes for monitoring the lipid order of biomembranes in live cells, J. Biochem. 170 (2021) 163–174, https://doi.org/10.1093/jb/mvab078.
[33] J. Zhang, C. Wang, L. Zhang, H. Wu, Y. Xiao, Y. Xu, X. Qian, W. Zhu, Novel nonplanar and rigid fluorophores with intensive emission in water and the application in two-photon imaging of live cells, RSC Adv. 6 (2016) 71624–71627, https://doi.org/10.1039/C6RA13226J.
[34] A.J. García-Sáez, D.C. Carrer, P. Schwille, Fluorescence Correlation Spectroscopy for the Study of Membrane Dynamics and Organization in Giant Unilamellar Vesicles, in: V. Weissig (Ed.), Liposomes, Humana Press, Totowa, NJ, 2010, pp. 493–508, https://doi.org/10.1007/978-1-60761-447-0_33.
[35] E. Sezgin, D. Waithe, J. Bernardino De La Serna, C. Eggeling, Spectral Imaging to Measure Heterogeneity in Membrane Lipid Packing, ChemPhysChem 16 (2015) 1387–1394, https://doi.org/10.1002/cphc.201402794.
[36] I. Urbančič, Z. Arsov, A. Ljubetič, D. Biglino, J. Štrancar, Bleaching-corrected fluorescence microspectroscopy with nanometer peak position resolution, Opt. Express 21 (2013) 25291, https://doi.org/10.1364/OE.21.025291.